Supporting Information

A metal free catalyst for efficient and stable one-step photocatalytic production of pure hydrogen peroxide

Hong Shi[a], Qingyao Wu[c], Zhenyu Wu[a], Yan Liu[a], Xiting Wang[a], Hui Huang*[a], Yang Liu*[a], Zhenhui Kang*[a,b]

[a] Institute of Functional Nano & Soft Materials (FUNSOM), Jiangsu Key Laboratory for Carbon-Based Functional Materials & Devices, Soochow University, 199 Ren'ai Road, Suzhou, 215123, China.

[b] Macao Institute of Materials Science and Engineering, Macau University of Science and Technology, Taipa 999078, Macau SAR, China.

[c] Key Laboratory of Chemical Biology of Hebei Province, College of Chemistry and Environmental Science, Hebei University, Baoding 071002, China.

*Correspondence: hhuang0618@suda.edu.cn; yangl@suda.edu.cn; zhkang@suda.edu.cn

Supplementary Text

1. The experimental method of transient photovoltage (TPV)

The TPV measurements were conducted under room temperature on platinum net covered with powder sample (1 cm × 1 cm) as the working electrodes and Pt wire as the counter electrodes. The *in-situ* TPV measurements were carried out under room temperature with indium-tin oxide (ITO) glass (1 cm × 2 cm) as the working electrodes and Pt wire as the counter electrodes. The working electrodes were prepared by depositing samples (100 μL, 2 mg mL^{-1}, dispersion liquid: 79.5% water, 20% isopropanol and 0.5% Nafion solution(v/v), respectively) on ITO glass substrates. During the testing process, the working electrodes were kept wet with anhydrous acetonitrile (or adding H_2O, N_2 saturated). The samples were excited by a laser radiation pulse (λ=355 nm, pulse width 5 ns) from a third-harmonic Nd: YAG laser (Polaris II, New Wave Research, Inc.). The photocurrent is the ratio of the photovoltage to the internal resistance of the test system.

2. Characterization

Powder X-ray diffraction (XRD) was employed to characterize the crystal structure of the as-prepared products by using a PIXcel3D X ray diffractometer (Empyrean, Holland Panalytical) with Cu Kα radiation (λ=0.154178 nm). The Fourier transform infrared (FTIR) spectra of the samples were performed with a Hyperion spectrophotometer (Bruker) with the scan range of 400–4000 cm^{-1}. High-resolution transmission electron microscopy (HRTEM) and transmission electron microscopy (TEM) were measured by using a FEI-Tecnai F20 transmission electron microscope with an accelerating voltage of 200 kV. X-ray photoelectron spectroscopy (XPS) measurements were carried on a KRATOS Axis ultra-DLD X-ray photo-electron spectroscope with a monochromatic Al Kα X-ray source (hv = 1486.6 eV). All electrochemical measurements were performed on a CHI 920C workstation (CH instruments, Shanghai, China), using a standard three electrode system, which are a

carbon electrode as the counter electrode, a saturated calomel electrode (SCE) as the reference electrode, and a glass carbon (GC) electrode as working electrode. The photoresponse-time curves under open circuit potential (OCP) were obtained in 0.1 M sodium sulfate (Na_2SO_4) solution with 100 W light-emitting diode (LED) lamp as light source. Electrochemical impedance spectra (EIS) measurements were carried out at open circuit potential as well, with a frequency range from 1 MHz to 0.01 Hz and Ac voltage amplitude of 5 mV in ultra-pure water. UV/VIS/NIR spectrophotometer (Lambda 750, Perkinelmer) was carried out to acquire the UV–Vis absorption spectra. TPV was measured on a home-made system. The TPV was excited with a nanosecond laser radiation pulse (wavelength of 355 nm and the repetition rate is 5 Hz) from a third harmonic Nd:YAG (Beamtech Optronics Co., Ltd). The signal of the TPV was amplified by the amplifier and recorded by the oscilloscope. All the measurements were performed at room temperature and under ambient pressure.

3. Electrochemical measurements for the determination of HOMO and LUMO

Cyclic voltammetry (CV) was operated using a standard three-electrode system with CHI 760E workstation (CH Instruments, Shanghai). A carbon electrode and an Ag/AgCl (3 M KCl) electrode were used as the counter electrode and the reference electrode, respectively. A glassy carbon (GC) electrode (3 mm diameter) was thoroughly cleaned by polishing to mirror finish, and dried before further use. 4 μL catalyst solution (2 mg mL^{-1}) and 5 μL of 0.5 wt % Nafion solution were dropped onto the working area of a cleaned GC electrode and put naturally to dry. The CV curves were measured in N_2-saturated 0.1 M BMIMPF6 solution with a scan rate of 50 mV s^{-1}. Ferrocene was added into the above solution as an internal standard with a concentration of 1 mg mL^{-1}. The HOMO and LUMO energy levels were calculated from the onset oxidation (E_{onset}^{OX}) reduction (E_{onset}^{RED}) potential and the reference energy level for ferrocene (4.8 eV below the vacuum level) as determined by CV according to the following equations:

$$E_{HOMO} = -\left(E_{onset}^{OX} - E_{Fc} + 4.8\right) eV \quad (1)$$

$$E_{LUMO} = -\left(E_{onset}^{RED} - E_{Fc} + 4.8\right) eV \quad (2)$$

Where E_{Fc} is the onset of the oxidation potential (vs. Ag/AgCl) of ferrocene.

4. Transient photocurrent responses (TPR) measurement

The TPR measurement was conducted with a three electrodes system. The test was performed at the open circuit potential with a 30-second light on/off cycle ($\lambda \geq 420$ nm). Typically, L-type glassy carbon electrode was used as the working electrodes, which was loaded with CQM-1, Quercetin-1, and Methyl bule-1 (100 μg cm^{-2}). The carbon rod was treated as the counter electrode and the saturated calomel electrode (SCE) was used as the reference electrode. The light was provided by a Xe lamp with a 420 nm filter.

5. Electrochemical impedance spectroscopy (EIS) measurement

The EIS was measured in a water solution with a three electrodes system at the open circuit potential. The glassy carbon electrode (GCE) coated with different catalysts (100 μg·cm^{-2}) was used as the working electrode. The carbon rod and saturated calomel electrode (SCE) were served as the counter electrode and the reference electrode. High frequency: 106 Hz, low frequency: 0.01 Hz.

6. Calculation of apparent quantum yield (AQY)

For AQY valuations, 10 mg photocatalyst, 15 mL ultra-pure water and a stir bar were put into a quartz photo-reactor vial with a total volume of 40 mL. Afterwards, the system was sealed and the vials were set under constant stirring with light-emitting diode (LED) applying a band-pass filter (λ_0=365, 420, 535 or 630 nm) for 1 h. The acidic potassium permanganate titration method was used to determine the amount of the generated hydrogen peroxide. The average intensity of irradiation was determined by an ILT 950 spectroradiometer (International Light Technologies) and the average

intensity of 365, 420, 535 and 630 nm irradiation were 32.23, 30.22, 1.52, 19.28 mW/cm^2, respectively and the irradiation area was 10.17 cm^2. The amount of H_2O_2 generated in 1 h of 365, 420, 535 and 630 nm irradiation are 61.8, 81.4, 3.0 and 40.7 μmol.

The number of incident photons (N) was calculated by Eq. (3)

$$N = {E\lambda}/{hc} \quad (3)$$

In Eq. (3), E is the average intensity of irradiation, λ stands for the wavelength (365, 420, 535 and 630 nm) of the irradiation, h represents the Planck (6.626×10^{-34} J·s = 4.136×10^{-15} eV·s) constant and c (3.0×10^{8} m·s^{-1}) is the speed of light.

The quantum efficiency was calculated from Eq. (4).

$$\mathrm{AQ}Y = \frac{2 \times \text{ number of evolved } H_2O_2 \text{ molecules}}{\text{number of incident photons}} \times 100\% \quad (4)$$

7. Determination of the electron transfer number

The electron transfer number was determined by rotating disk-ring electrodes (RRDE) testing system (RRDE-3, ALS Co., Ltd). To determine the electron transfer number of photocatalytic oxygen reduction reaction, RRDE experiment was carried out in ultrapure water (O_2 saturated) with a scan rate of 10 mV s^{-1} and rotating speed of 1600 rpm. The disk potential was set at open circuit potential to avoid photochemical and electrochemical catalysis process for water oxidation. For photocatalytic water splitting, RRDE experiments were conducted in ultrapure water (N_2 saturated) with a scan rate of 10 mV s^{-1} and rotating speed of 1600 rpm. The disk potential was set at a positive bias potential to avoid the oxygen reduction reaction. The ring potential was kept at 0.9 V vs. SCE, which can oxidize the generated H_2O_2 from the disk into O_2. All the process and data were collected by a CHI 760E electrochemical workstation (CH Instruments, Shanghai, China), using carbon electrode and saturated calomel electrode (SCE) as the counter electrode and the reference electrode, respectively.

$$n = \frac{4\Delta I_{disk}}{\Delta I_{disk} + {\Delta I_{ring}}/{N}} \quad (5)$$

where $^{\Delta}I_{ring}$ is the current of ring electrode, $^{\Delta}I_{disk}$ is the current of disk electrode, which test in four electrode system in H_2O electrolyte, with 1600 rpm rotate speed.

Supplementary Figures

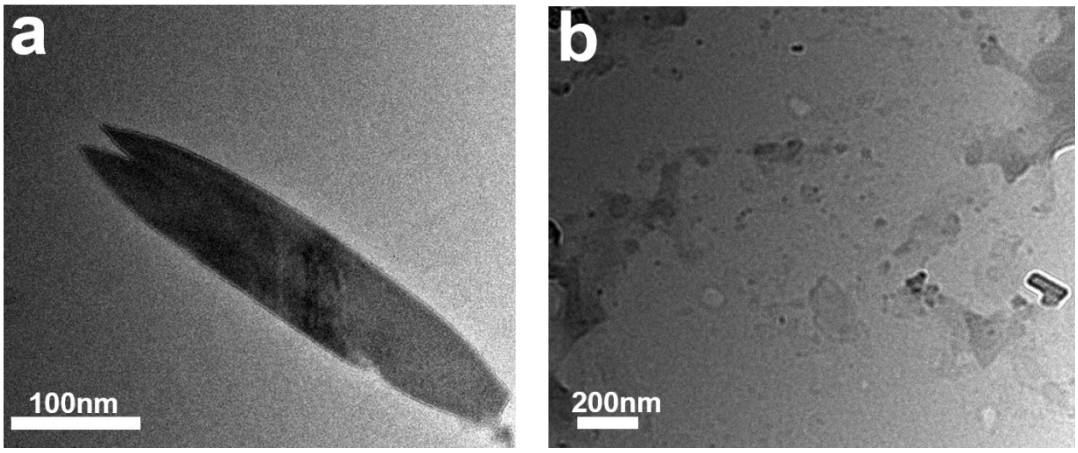

Fig. S1. (a) TEM image of Quercetin-1. (b) TEM image of Methyl blue-1.

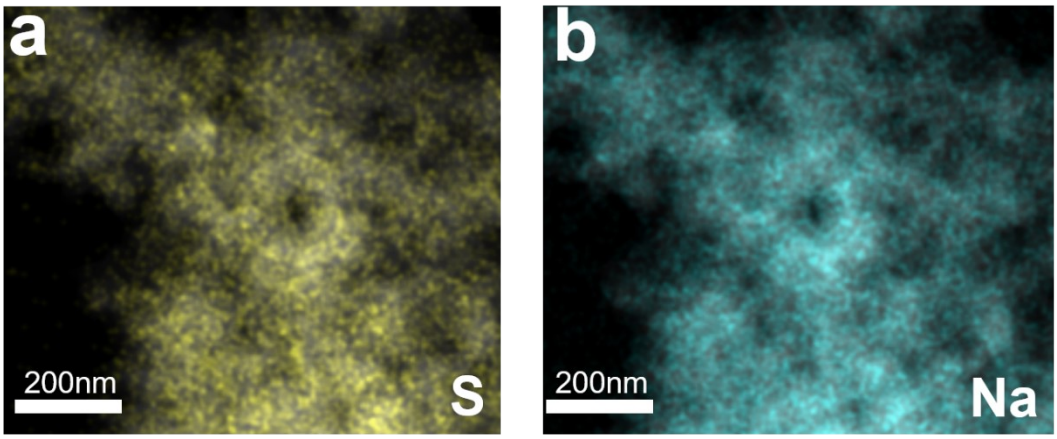

Fig. S2. The mapping images for (a) S and (b) Na elements of CQM-1.

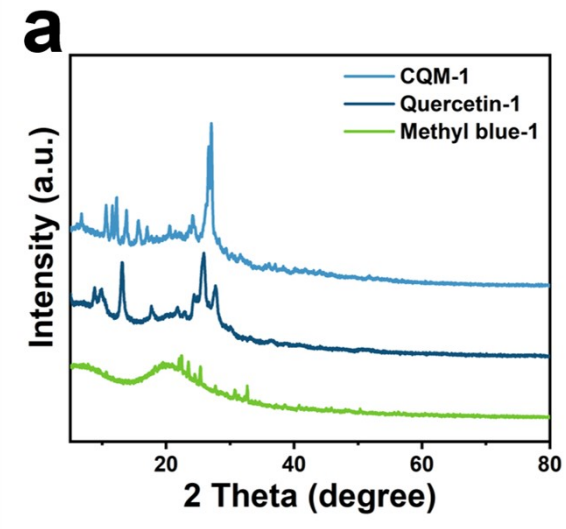

Fig. S3. XRD patterns of CQM-1, Quercetin-1 and Methyl blue-1.

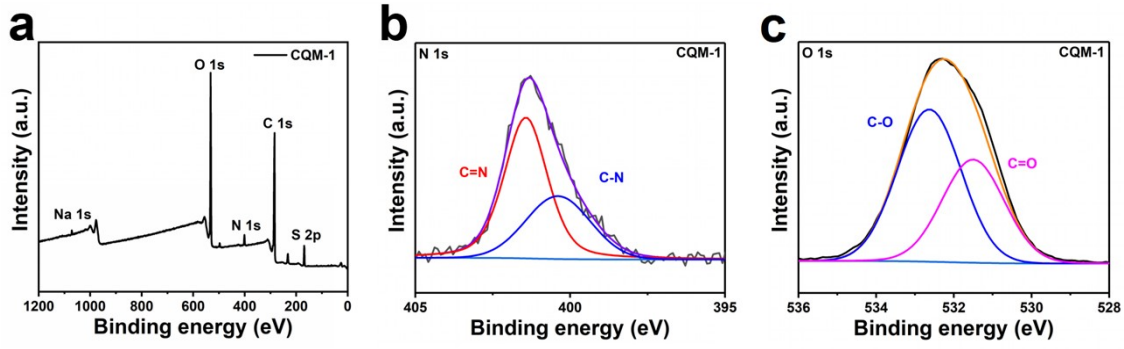

Fig. S4. XPS survey spectrum (a) and high-resolution XPS spectra of CQM-1: (b) O 1s and (c) N 1s.

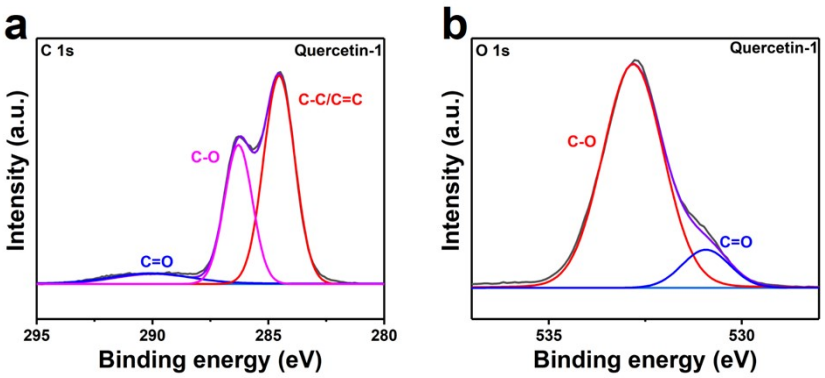

Fig. S5. High-resolution XPS spectra of Quercetin-1: (a) C 1s and (b) O 1s.

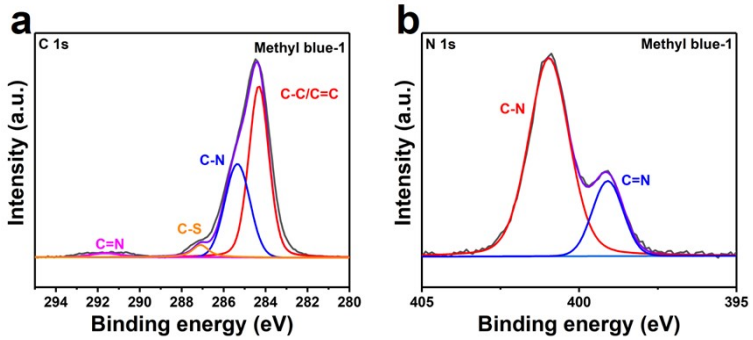

Fig. S6. High-resolution XPS spectra of Methyl blue-1: (a) C 1s and (b) N 1s.

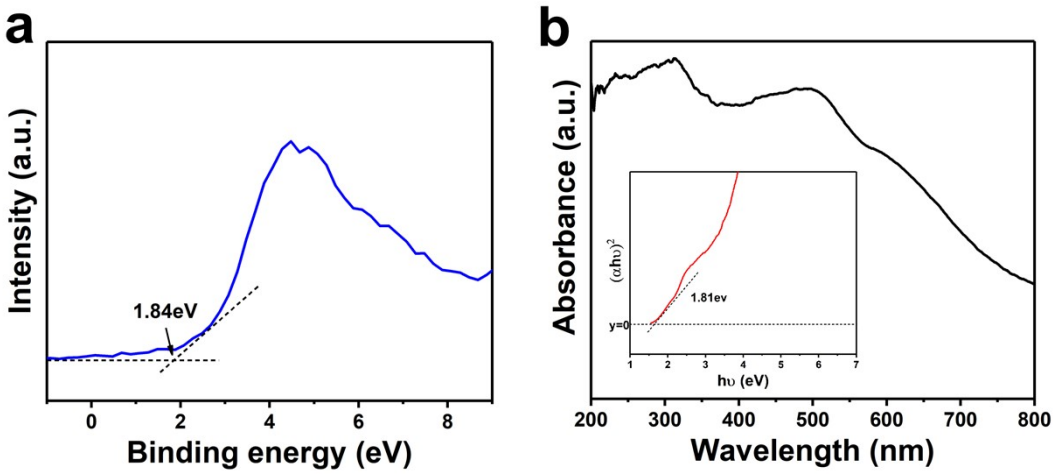

Fig. S7. (a) VB state of CQM-1 measured by XPS spectroscopy. (b) UV-Vis absorption spectrum of CQM-1 (inset is the corresponding Tauc plot).

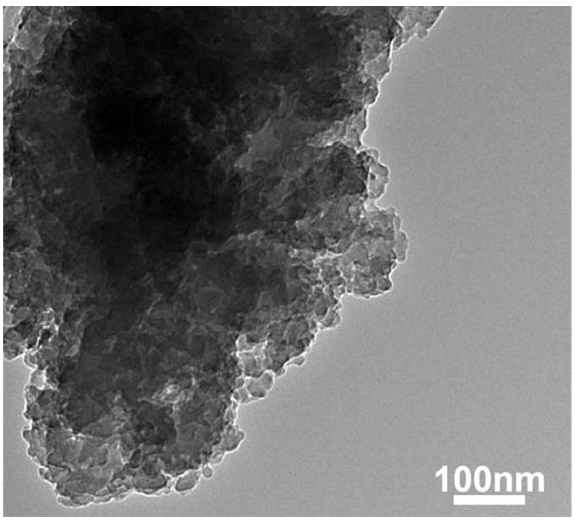

Fig. S8. TEM image of CQM-1 after five cycles.

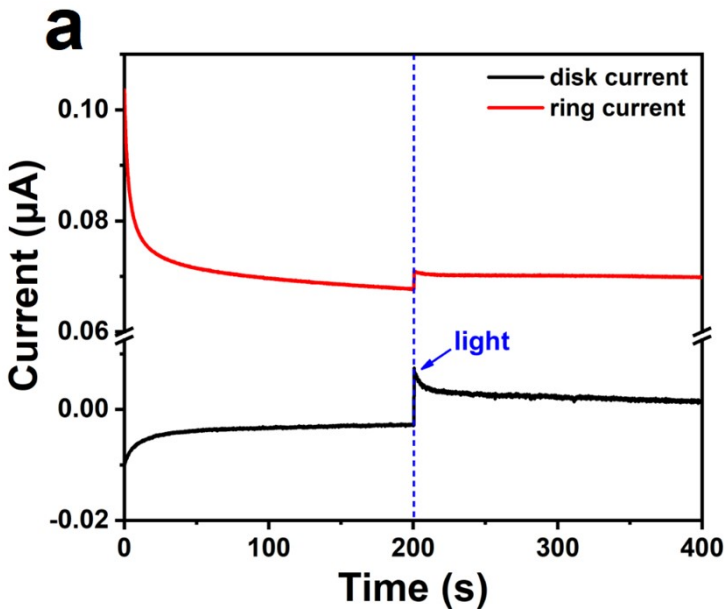

Fig. S9. The electron transfer number (n) during the photocatalytic reaction of CQM-1.

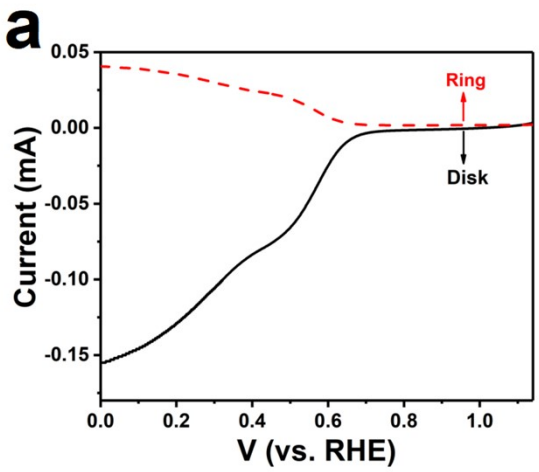

Fig. S10. Rotating ring-disk electrode (RRDE) voltammograms obtained in 0.1M Na_2SO_4 solution (pH=7) with a scan rate of 10 mV s^{-1} and a rotation rate of 1,600 r.p.m.. The oxidation current observed during RRDE tests indicates the oxidation of H_2O_2 occurs at the ring electrode.

Supplementary Tables

Table S1. Elemental compositions of samples from XPS results.

Sample	Contents (at. %)				
	C	N	Na	O	S
CQM-1	60.59	3.42	0.46	31.36	4.18
Quercetin-1	71.32	/	/	28.68	/
Methyl blue-1	51.86	1.07	11.2	33.93	1.95

Table S2. List of electron attenuation constants (τ), the maximum extraction rate (t_{max}) of charge and the maximum charge extraction efficiency (A) of CQM-1, Quercetin-1 and Methyl blue-1.

Sample	τ	t_{max}	A	$n_e=A*\tau/t_{max}$
CQM-1	0.443	0.085	0.185	0.964
Quercetin-1	0.164	0.008	0.062	0.127
Methyl blue-1	0.186	0.043	0.016	0.069

Table S3. The AQY values with different incident light wavelengths.

Wavelength (nm)	Light intensity ($mW \cdot cm^{-2}$)	$n_{H_2O_2}$ (μmol)	AQY (%)
365	32.23	61.8	4.33
420	30.22	81.4	5.30
535	1.52	3.0	3.05
630	19.28	40.7	2.77

Table S4. ICP-MS of CQM-1, Quercetin-1 and H_2O_2 product.

	ICP-MS results (at. %)									
	Fe	Co	Ni	Cu	Mn	Al	K	Mg	Ca	Zn
CQM-1	BDL	BDL	BDL	BDL	BDL	BDL	BDL	BDL	BDL	BDL
Quercetin-1	BDL	BDL	BDL	BDL	BDL	BDL	BDL	BDL	BDL	BDL
H_2O_2 solution	BDL	BDL	BDL	BDL	BDL	BDL	BDL	BDL	BDL	BDL

BDL: below detection limit.

Table S5. Recent studies reported for the use of photocatalysts in H_2O_2 production.

Catalyst	Scavenger	H_2O_2 Production μmol g^{-1} h^{-1}	Cycle	Ref.
CQM-1	/	3676	5	**This work**
CoP/Co@NPC-15/g-C_3N_4	Isopropanol (IPA)	940	3	[S1]
CNK0.2 w	Methanol	1010	/	[S2]
C_3N_4/AQ	Organic electron donor (2-propanol)	361	/	[S3]
PEI/C_3N_4	/	208.1	/	[S4]
g-C_3N_4/MTI49	/	22.9	/	[S5]
Au/C_3N_4	C_2H_5OH	168	/	[S6]
CPN	/	1968	/	[S7]
PIx-NCN	Methanol	1240	10	[S8]
$Cu_2(OH)_2CO_3$/g-C_3N_4	/	1277		[S9]
K^+ and Na^+ are doped into g-C_3N_4	/	375		[S10]
Graphene oxide	/	666	/	[S11]
BP/g-C_3N_4	Isopropanol	540	/	[S12]
CdS/rGO	Isopropanol	213.4	/	[S13]

References:

[S1] Q. Ji, L. Pan, J. Xu, C. Wang and L. Wang, *ACS Appl. Nano Mater.*, 2020, **3**, 3558–3567.

[S2] Y. Wang, D. Meng and X. Zhao, *Appl. Catal. B-Environ.*, 2020, **273**, 119064.

[S3] H. Kim, Y. Choi, S. Hu, W. Choi and J.-H. Kim, *Appl. Catal. B-Environ.*, 2018, **229**, 121–129.

[S4] X. Zeng, Y. Liu, Y. Kang, Q. Li, Y. Xia, Y. Zhu, H. Hou, M.H. Uddin, T.R. Gengenbach, D. Xia, C. Sun, D.T. Mccarthy, A. Deletic, J. Yu and X. Zhang, *ACS Catal.*, 2020, **10**, 3697–3706.

[S5] Y. Kofuji, S. Ohkita, Y. Shiraishi, H. Sakamoto, S. Ichikawa and S. Tanaka, *T. Hirai, Eng.*, 2017, **5**, 6478–6485.

[S6] G. Zuo, S. Liu, L. Wang, H. Song, P. Zong, W. Hou, B. Li, Z. Guo, X. Meng, Y. Du, T. Wang and V.A.L. *Roy, Catal. Commun.*, 2019, **123**, 69–72.

[S7] J. Cao, H. Wang, Y. Zhao, Y. Liu, Q. Wu, H. Huang, M. Shao, Y. Liu and Z. Kang, *J. Mater. Chem. A*., 2020, **8**, 3701–3707.

[S8] L. Yang, G. Dong, D.L. Jacobs, Y. Wang, L. Zang and C. Wang, *J. Catal.*, 2017, **352**, 274–281.

[S9] Z. Li, N. Xiong and G. Gu, *Dalton Trans.*, 2019, **48**, 182–189.

[10] X. Qu, S. Hu, J. Bai, P. Li, G. Lu and X. Kang, *J. Mater. Sci. Technol.*, 2018, **34**, 1932–1938.

[S11] Y. Kofuji, S. Ohkita, Y. Shiraishi, H. Sakamoto, S. Tanaka and S. Ichikawa, *T. Hirai, ACS Catal.*, 2016, **6**, 7021–7029.

[S12] Y. Zheng, Z. Yu, H. Ou, A.M. Asiri, Y. Chen and X. Wang, *Adv. Funct. Mater.*, 2018, **28**, 1705407.

[S13] S. Thakur, T. Kshetri, N.H. Kim and J.H. Lee, *J. Catal.*, 2017, **345**, 78–86.